# Development of probabilistic risk assessment methodology against strong wind hazards in floating nuclear power plants - Part I: hazard assessment

Lan-Xin Gong,[1] Qing-Zhu Liang,[2] Hang Zhang,[3] and Chang-Hong Peng[1,*]

[1]*School of Nuclear Science and Technology, University of Science and Technology of China, Hefei 230026, China*
[2]*Institute of Plasma Physics, Hefei Institutes of Physical Science, Chinese Academy of Sciences, Hefei 230031, China*
[3]*Nuclear Power Institute of China, Chengdu 610213, China*

This study introduces a probabilistic risk assessment (PRA) framework against evaluating extreme wind hazards on floating nuclear power plants (FNPPs), extending conventional land-based nuclear plant methodologies through wind speed-based hazard curve development. We establish an integrated analytical approach incorporating 1) multi-source meteorological data integration, 2) coupled wind field modeling with extreme value theory, and 3) Bayesian uncertainty quantification. Hazard curves were systematically derived for three wind phenomena – straight-line winds, typhoons, and tornadoes – with consideration of their combination. The methodology advances inverse uncertainty quantification through Markov Chain Monte Carlo (MCMC) parameter calibration for typhoon and straight-line wind models, enabling probabilistic propagation of parameter uncertainties into hazard estimates. Tornado risk assessment integrates stochastic encounter modeling with classification error-adjusted conditional probabilities, enhanced through Bayesian updating techniques. Key findings reveal substantial epistemic uncertainties in low-probability hazard regions, primarily attributable to data sparsity in extreme wind records and empirical limitations of current wind field parameterizations. This work establishes a foundational methodology for marine nuclear infrastructure risk assessment while highlighting critical knowledge gaps in extreme wind characterization for floating systems.

Keywords: Floating nuclear power plant (FNPP), Strong wind hazard, PRA, MCMC

## I. INTRODUCTION

Floating nuclear power plants (FNPPs) integrate nuclear reactors into floating offshore platforms, representing an innovative nuclear energy system characterized by modular construction, flexible deployment, and strong environmental adaptability [1, 2]. FNPPs are particularly suited for remote islands, offshore oil and gas fields, and coastal energy supply. However, the complex marine environment presents unique safety challenges, necessitating systematic safety analyses to ensure secure and reliable operation. The unique safety concerns of FNPPs stem from the coupling effects between the marine environment and nuclear systems. These include: (1) dynamic external hazards such as extreme meteorological events (strong winds [3], sea ice [4], snowfall [5], earthquakes [6], tsunamis [7]) and external impact events like ship collisions [8]; (2) thermal-hydraulic variations caused by marine motions (e.g., inclination, rolling, heaving) and the long-term environmental effects on structural and system components [9, 10]; and (3) the complex dispersion behavior of radioactive materials in the ocean-atmosphere interface [11].

Several safety assessment methodologies have been employed for FNPPs. Deterministic safety analysis primarily focuses on design-basis accident (DBA) scenarios, employing thermal-hydraulic simulations to evaluate system responses under predefined accident conditions. System codes adapted for marine applications, such as MARS-KS and RELAP5, have validated natural circulation and two-phase flow characteristics under marine motion conditions [12, 13]. Structural integrity assessments have also been conducted to evaluate FNPPs' resistance to external loads and environmental stresses [14]. In parallel, accident mitigation strategies have been investigated to enhance the resilience of safety-critical systems [15].

Probabilistic safety assessment (PSA) quantifies accident frequencies and consequences, identifying key risk factors and serving as a fundamental tool for FNPP safety evaluation. Existing PSA research has primarily focused on human reliability analysis [16–18], system reliability evaluation, and accident consequence assessment [5, 8, 19]. Additionally, some studies have explored mission safety for floating nuclear-powered vessels [20]. Despite these efforts, PSA studies specifically addressing extreme wind hazards for FNPPs remain limited. Izmail Kantarzhi [21] estimated the probability of extreme wave events occurring once in 10,000 years using the annual maximum method applied to storm data from 1991 to 2021. The peak distribution was approximated using the Generalized Extreme Value (GEV) distribution in its Weibull form. The SWAN model was utilized for wave modeling, while wind field calculations were based on NCEP/NCAR reanalysis data from 1991 to 2021.

Current PSA methodologies for extreme wind conditions primarily derive from land-based nuclear power plant (NPP) studies. For long-duration straight-line winds (distinct from typhoons and tornadoes), Hiroyuki Nishino et al. [22] developed a PRA model for sodium-cooled fast reactors. Using Weibull and Gumbel distributions derived from Japanese meteorological data, they estimated wind risk curves and identified critical structures and components essential for decay heat removal. An event tree analysis assessed core damage potential, considering wind-induced loads and airborne debris hazards (e.g., steel pipes, beams, vehicles, and trees). Subsequently, Hidemasa Yamano et al. [23] extended this PRA framework to account for combined strong wind and heavy rainfall events. Their model incorporated maximum instanta-

* Corresponding author, pengch@ustc.edu.cn

neous wind speeds, hourly precipitation, and rainfall duration to derive hazard curves and event sequences associated with compound disasters.

For tornado hazards, Nishino et al. [24] estimated the annual probability of tornado occurrence at selected NPP sites based on historical tornado data. They employed the Weibull distribution to calculate maximum wind speeds' exceedance probability and constructed tornado hazard curves. Another study [25] refined tornado hazard assessments using the Fujita scale, integrating a windborne debris impact model to quantify the frequency of damage to critical plant components. Further research [26] incorporated tornado hazards into internal event models by modifying event and fault trees to evaluate tornado contributions to core damage frequency.

Typhoon risk assessments are mainly conducted using numerical simulations based on physical models of typhoon wind fields for typhoon hazards. These models, including those developed by Batts et al. [27] and Vickery et al. [28], typically comprise submodels for typhoon trajectory prediction, central pressure evolution, and wind field characteristics. Detailed methodologies can be found in [29]. The aerodynamic modeling of typhoon debris impact on safety-related structures, systems, and components (SSCs) follows similar principles to tornado risk assessment. However, unlike tornado wind fields, typhoon wind field models incorporate height-dependent horizontal wind speed variations [30, 31].

This study introduces a probabilistic safety assessment (PSA) methodology tailored for floating nuclear power plants (FNPPs) exposed to extreme wind hazards, addressing critical gaps in existing terrestrial nuclear plant frameworks through marine-specific adaptations. Three principal modifications differentiate the proposed approach: (1) Revised hazard characterization accounting for sustained typhoon intensification over open waters, contrasting with terrestrial wind field attenuation post-landfall. (2) Implement multiphysics coupling analysis to evaluate synergistic wind-wave interactions that threaten structural integrity and platform stability. (3) Redefined windborne debris models reflecting FNPP-specific configurations and containment designs that inherently mitigate seawater intrusion risks.

The methodology enhances PSA through uncertainty analysis, integrating inverse uncertainty quantification for empirical model parameter calibration and Bayesian updating of sparse meteorological inputs. This dual approach strengthens hazard curve reliability while establishing rigorous uncertainty bounds, which is crucial given the limited historical typhoon data in prospective FNPP deployment zones. By reconciling marine environmental dynamics with nuclear safety requirements, the framework provides a foundation for risk-informed design and operational decision-making for offshore nuclear installations.

## II. METHODOLOGY

### A. Analysis Framework

Drawing on the external hazard assessment process used for land-based nuclear power plants, we propose an analytical framework tailored to floating nuclear power plants, as illustrated in Fig. 1. The framework consists of three main components: strong wind hazard analysis, SSC vulnerability assessment, PSA modeling and quantitative evaluation. The framework is consistent with the external event probabilistic safety analysis of both light and non-light water reactors. However, due to the unique deployment environments of floating platforms, additional attention is required to address the specific hazard analysis associated with wind-generated waves. This paper focuses on the strong wind hazard analysis, situated at the foundational level of the proposed analytical framework. In addition to wind-generated waves, this article does not consider the coupled situations of strong winds with other disasters (such as lightning and heavy precipitation).

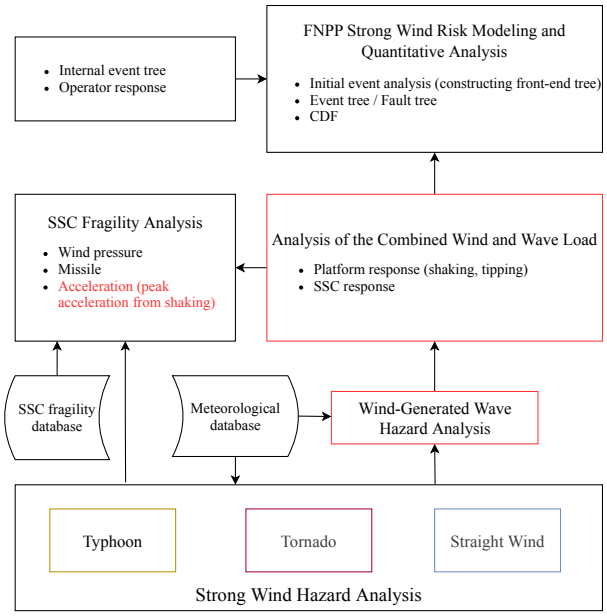


Fig. 1. Analytical framework for the probabilistic risk assessment of floating nuclear power plants against strong wind hazard.

### B. Strong Wind Hazard Analysis

#### 1. *Typhoon*

A typhoon (or hurricane) is an intense tropical cyclone. It is usually assumed that the occurrence of typhoons follows a Poisson distribution, and that the wind speed exceedance events from different tropical cyclones within a given year are mutually independent, the annual exceedance probability for the extreme wind speed $v$ at the specified plant site can be

determined using the following model [27].

$$P(V > v, \tau = 1) = 1 - \sum_{n=0}^{\infty} F_v^n \frac{(\lambda\tau)^n}{n!} e^{-\lambda\tau} = 1 - e^{-\lambda(1-F_v)} \tag{1}$$

where $\lambda$ denotes the average number of typhoons occurring annually, and $F_v$ denotes the probability that a single typhoon will produce extreme wind speeds not exceeding $v$ at the plant site location.

The parameter $\lambda$ can be derived from statistical data. The exceedance probability $F_v$ can be estimated using the Monte Carlo (MC) simulation method. The wind field model applied is the Batts wind field, and the primary steps are as follows:

1. Typhoon key parameters are sampled based on the probabilistic model of typhoon key parameters in the plant site area, including the difference pressure between the center and periphery of the typhoon $\Delta P_{max}$, the radius of the maximum wind speed $R_{max}$, the translational velocity $V_T$, the angle of the direction of movement $\theta$, the minimum distance from the study point $D_{min}$, and the angle of the typhoon movement analysis with the initial angle $\alpha_0$ of the plant site.

2. Calculate the wind speed sequence generated by the tropical cyclones simulated using the Batts typhoon wind field model at the site location.

3. Record the extreme wind speeds produced by the simulated tropical cyclones at the site location.

4. Repeat steps 1 and 2 until the specified sample size $m$ is reached, thereby obtaining $m$ extreme wind speeds generated by $m$ simulated tropical cyclones at the site location. Subsequently, estimate $F_v$ using Eq. (2).

$$F_{v_i} = \frac{i}{m+1} \tag{2}$$

where $v_i$ denotes the extreme wind speed generated by the $i-$th simulated tropical cyclone at the plant site location.

Fitting meteorological data can provide the input for the above steps, specifically the probabilistic model of key typhoon parameters tailored to the plant site. A standard method for simulating this model involves selecting tropical cyclones as samples that pass through a circular area with a radius of 250 kilometers centered on the study point. This approach is typically employed in the statistical analysis of tropical cyclones affecting nuclear power plants, facilitating distribution fitting and hypothesis testing.

As the cornerstone of the Monte Carlo (MC) simulation, the Batts model is selected for its maturity, reliability, minimal input parameter requirements, and computational efficiency. Fig. 2 shows the geometric relationship between the primary input parameters of the model. Point O represents the center position of the current typhoon, and its distance from the factory site (research point) is $R$. As mentioned previously, $R$ should be less than 250 kilometers.

The physical models incorporated in the Batts model include the maximum gradient wind speed of hurricanes, the wind speed height distribution, and the intensity decay model. The maximum gradient wind speed of the typhoon $V_{gx}$ is determined by,

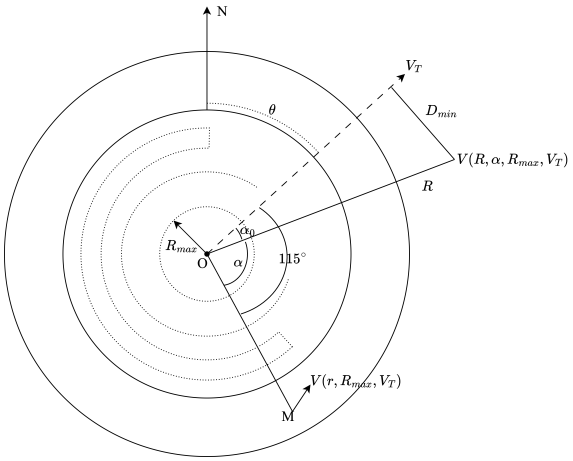


Fig. 2. Batts wind model illustration

$$V_{gx} = -\frac{R_{max} f}{2} + \left(\frac{R_{max}}{\rho}\frac{\mathrm{d}p}{\mathrm{d}n}\right)^{0.5} = -\frac{R_{max} f}{2} + \alpha(\Delta P_{max})^{0.5} \tag{3}$$

where $f$ is the Coriolis parameter. $\rho$ is the density of air. $\alpha$ is an empirical parameter with a value of 6.95.

The maximum wind speed at 10 m above the ocean surface, averaged over 10 minutes, is assumed to be given by the empirical relation

$$V(z = 10, R_{max}) = 0.865 V_{gx} + 0.5 V_T \tag{4}$$

Let the center of the storm be denoted by O, and let a line OM be defined that makes an angle of 115° clockwise from the direction of motion of the storm. The 10-min wind speed at 10 m above the ocean surface at a distance $r$ from 0 along the line OM is denoted by $V(z = 10, r)$.

$$\frac{V(z = 10, r)}{V(z = 10, R_{max})} = \begin{cases} \frac{r}{R_{max}}, r \le R_{max} \\ \left(\frac{R_{max}}{r}\right)^k, r > R_{max} \end{cases} \tag{5}$$

where $k$ is the exponent of the power-law distribution, with a base value of 0.6. As the meteorological data usually records the typhoon's 6th-grade wind radius $R_6$ and central pressure $p_{min}$, the maximum wind speed radius $R_{max}$ is usually calculated using the following formula,

$$V_m = K(1010 - p_{min})^n \tag{6}$$

$$R_{max} = (10.8/V_m)^{(1/k)} R_6 \tag{7}$$

where $K$ and $n$ are empirical coefficients with benchmark values of 3.059 and 0.644, respectively [32].

Let the angle between a line ON and line OM be denoted by $\theta$. The 10-min wind speed $V(z = 10, r, \theta)$ at 10 m above the surface at a distance $r$ from the storm center on line ON is assumed to be given by the expression,

$$V(z=10,r,\theta)=V(z=10,r)-\frac{V_T}{2}(1-\cos\theta) \quad (8)$$

The decay of typhoon intensity with time is characterized using the decay of the pressure difference between the center and the periphery,

$$\Delta p(t)=\Delta P_{\max}-0.02(1+\sin\phi)t \quad (9)$$

where $t$ is the time experienced by the typhoon (in hours), $\Delta p(t)$ is the pressure difference between the center and the periphery, and $\phi$ is the angle between the coast where the plant site is located and the track of the typhoon.

The following formula converts the calculated 10-minute average maximum wind speed to the extreme wind speed (3-second gust wind speed at 10m height).

$$U_t(z)=U(z)\left[1+\frac{\sqrt{\beta\,(z,z_0)}c(t)}{2.5\ln\left(z/z_0\right)}\right] \quad (10)$$

where $U(z)$ is the velocity $V(z=10,r,\theta)$ at time $t$. $z$ represents height, with a value of 10m. $z_0$ is the surface roughness, and the results of $\beta(z,z_0)$ and $c(t)$ are given in tabular form. Because floating platforms are deployed in more open water, a smaller surface roughness ($z_0=0.005$m) was selected, which differs from land-based nuclear power plants. Further details can be found in reference [33].

### 2. *Tornado*

Tornadoes are a type of severe weather phenomenon different from typhoons, with a shorter duration and difficulty to predict. Tornado records are usually expressed by the Fujita scale and subsequent enhanced Fujita scale, and the annual wind speed exceedance probability of all Fujita-scale tornadoes is typically calculated as [34],

$$P_{T=1}(V>v)=1-\exp\left[-\nu_{avg}\sum_{i=0}^{F_{max}}P(V>v|F_i)P(F_i)\right] \quad (11)$$

where $\nu_{avg}$ is the average occurrence rate of tornadoes of different Fujita scales. $F_{max}$ indicates the maximum F-scale intensity of a tornado. Assuming the location where a tornado occurs within a region is uniformly distributed, $P(V>v|F_i)$ can be calculated as,

$$P(V>v|F_i)=\begin{cases}\frac{A_0}{S}, if \quad A_0\le S\\ 1, \quad otherwise\end{cases} \quad (12)$$

where $S$ denotes the area of the statistical tornado used to calculate $\nu_{avg}$ and $A_0$ denotes the tornado source area.

$$A_0=L_t^*W_t^* \quad (13)$$

Tornado wind speeds exceeding the path length $L_t^*$ and path width $W_t^*$ can be estimated using the Monte Carlo simulation of the Rankine tornado wind field [35], with the main steps as follows,

1. Based on the probability distributions of the tornado path length $L_t$, maximum horizontal wind speed $U_{max}$, the ratio of tangential to radial wind speed $\gamma$, and the radius of maximum wind speed $R_{max}$ under a specific $F_i$ intensity, random sampling is conducted to obtain the parameters mentioned above.

2. The path length $L_t$ is then corrected to yield the effective path length $L_t^*$ that exceeds the wind speed $v$.

3. Using the tornado wind field parameters $U_{max}$ , $\gamma$, and $R_{max}$, the path exceedance width $W_t^*$ beyond the wind speed $v$ is calculated, assuming the tornado translational speed $U_T=U_{max}/5$ [33].

4. Steps 1–3 are repeated until the specified sample size is reached, and the Monte Carlo method is applied to estimate the mean values of the path length $L_t^*$ exceeding the wind speed $v$ and the path exceedance width $W_t^*$.

The estimated values of $L_t^*$ and $W_t^*$ for different $F_i$-level intensities obtained through the above process, along with the computed exceedance area of wind speed $(\hat{A}_0^*)_k$ for different $F_i$-level intensities, allow the annual exceedance probability of tornado wind speed to be estimated as [36],

$$P_{T=1}(V>v)=1-\exp\left[\nu_{avg}\sum_{k=0}^{F_{max}}\frac{\left(\hat{A}_0^*\right)_k}{S}P(F_k)\right] \quad (14)$$

$$P(F_k)=\frac{n_k}{n_t} \quad (15)$$

$$\ln n_i=au_i+b \quad (16)$$

where $n_k$ represents the number of tornado occurrences at level $k$, and $n_t$ represents the total number of tornado occurrences. $n_i$ is the cumulative number of tornadoes with maximum wind speeds exceeding some threshold wind speed, and $u_i$ is the threshold wind speed at the $F_i$ intensity level. $a$ and $b$ are the least squares coefficients of $\ln n_i$ and $u_i$.

### 3. *Straight-line wind*

Unlike typhoons and tornadoes, straight-line winds typically do not have models that directly describe them. Their annual exceedance frequency is usually obtained through fitting an extreme value distribution.

The cumulative probability of the $i$-th extreme wind speed is calculated using the following equation, assuming that the annual extreme wind speeds for $N$ consecutive years are ordered from smallest to largest.

$$F(V_i)=\frac{i-\alpha}{N+1-2\alpha} \quad (17)$$

where $\alpha$ is taken as 0.4 according to the Cunnane criterion. Type I (Gumbel distribution) and Type III extreme value distributions (Weibull distribution) extreme value distributions were fitted to obtain the annual exceedance frequencies for straight-line winds [37].

$$F(X) = \exp\left\{-\exp\left[-\left(\frac{X-\mu}{\theta}\right)\right]\right\}$$
$$F(X) = 1 - \exp\left[-\left(\frac{X}{\eta}\right)^{m}\right] \quad (18)$$

where $X$ represents the wind speed (m/s). $\mu$ is the location parameter of the Gumbel distribution. $m$ is the shape parameter of the Weibull distribution. $\theta$ and $\eta$ are the scale parameters.

#### 4. *Combined wind*

Given the significant differences in the meteorological origins of various wind disasters, it can be assumed that the wind speed exceedance events associated with different types of wind disasters are statistically independent. Consequently, the annual exceedance probability of combined wind hazards from all potential strong wind disaster types in the plant site area can be estimated using the following formula.

$$P(V > v) = 1 - \prod_{i=1}^{s}[1 - P(V_i > v)] \quad (19)$$

where $P(V > v)$ denotes the annual exceedance probability of the combined wind, $s$ is the number of strong wind hazard types considered, and $P(V_i > v)$ is the annual exceedance probability of the $i$-th strong wind hazard type.

### C. Uncertainty Analysis

Due to the high uncertainty inherent in meteorological data and models, the results of strong wind hazard analyses also exhibit significant uncertainty. In the context of typhoon hazard analysis, considering the maturity of wind field models and the completeness of observational data, the uncertainty associated with the input parameters of the Batts model can be quantified through fitting meteorological data. Additionally, by correlating the extreme wind speeds observed at corresponding stations during typhoon events with the typhoon wind field model, key parameters of the Batts model can be calibrated and subjected to inverse uncertainty quantification (UQ). The Markov Chain Monte Carlo (MCMC) method is employed as the core tool for inverse uncertainty quantification [38]. The typical Metropolis-Hastings algorithm is described as follows.

Listing 1. Metropolis-Hastings for Inverse UQ

```
Input: Likelihood function L(y|θ), Prior P(θ),
    Proposal Q(θ'|θ), Initial guess θ_0, Number of
    samples N

θ ← θ_0
Compute P_θ = L(y|θ)P(θ)
Initialize empty sample list

for i = 1 to N do
    Propose θ' ~ Q(θ'|θ)
    Compute posterior probability P_θ' = L(y|θ')P(θ')
    Compute acceptance ratio α = min(1, P_θ'/P_θ)
    Sample u ~ Uniform(0, 1)
    if u < α then
        θ ← θ'
        P_θ ← P_θ'
    end if
    Append θ to samples
end for

Return: samples
```

In listing 1, to simplify the process, the proposed distribution $Q$ satisfies $Q(\theta'|\theta) = Q(\theta|\theta')$.

Similarly, for straight-line winds, although no wind field model is used for direct characterization, the sufficient availability of statistical data allows for inverse uncertainty quantification of the parameters of Gumbel and Weibull distributions based on observational data. The resulting uncertainty distribution of model parameters is then propagated forward to quantify the uncertainty in the hazard curve.

Tornadoes are unique because current meteorological records primarily consist of qualitative descriptions of their destructive impacts, requiring manual conversion into Fujita or Enhanced Fujita (EF) scales for analysis. Significant uncertainties exist in data sources, wind speed distribution, occurrence rates, and path length and width. Due to the lack of direct observational data, a probabilistic encounter model and a tornado intensity estimation model [39] are employed to quantify uncertainties in data sources, wind speed distribution, and occurrence rates, while path length and width are sampled in the Monte Carlo (MC) simulation. The probabilistic encounter model gives the probability matrix $P^{e}_{k,i}$ for a tornado with a maximum magnitude of $F_k$ but a magnitude of $F_i$ at observation. The tornado intensity estimation model provides the coefficient of variation between the estimated speed and the actual speed. Using Bayes' formula, an accurate tornado rating can be inferred from the current tornado statistical data.

$$P(F_i^T|F_j^O) \propto P(F_i^O|F_j^T)P(F_j^T) \quad (20)$$

where $F_i^T$ is the actual tornado intensity, and $F_j^O$ is the tornado intensity inferred from damage.

## III. CASE STUDY

### A. Data Collection

We have collected relevant meteorological data to potentially deploy a floating nuclear power plant off the coast of Yantai (37.4°N, 121.4°E). The assessment of typhoons is based on the CMA best track dataset (1949–2023) and satellite-derived tropical cyclone-scale data (1980–2016) from the China Meteorological Administration's tropical cyclone data center (tcdata.typhoon.org.cn) [40, 41]. ERA5

hourly surface data (1950 to present) is used for calibrating model parameters [42].

Meteorological data on tornadoes are obtained from reference [36] (1950–2003), reference [43] (2004-2014), and reference [44] (2003-2019).

Historical weather data for Yantai have been collected from https://zh.weatherspark.com for straight-line winds. Annual maximum gust wind speeds have been statistically analyzed from 1973 to 2020.

## B. Hazard Curve and Uncertainty Analysis

### 1. *Typhoon*

Tropical cyclones with trajectories passing through a circular region with a 250 km radius centered on the study site were selected as samples. The dataset of tropical cyclones affecting the specific plant site was statistically analyzed to estimate the probabilistic model of key parameters for tropical cyclones in the region. The results are presented in the Fig. 3.

After the K-S hypothesis test, the probability models of the typhoon wind field input parameters are shown in Table 1. Since the number of samples is not too large, there is a certain bias in the fitting, and the fitted parameterized distributions are selected for all parameters except the empirical distribution of the typhoon's moving direction angle $\theta$, which helps the subsequent MC simulations to produce higher extreme wind speeds.

Table 1. Distribution of input parameters for the Batts wind field model

| Parameters | Distribution | Distribution parameters |
|---|---|---|
| $\lambda$ | Possion | $\nu = 0.68$ |
| $\Delta P_{max}$ | Weibull | $m = 2.434, \eta = 18.152$ |
| $R_{max}$ | Gumbel | $\mu = 49.411, \theta = 8.425$ |
| $V_T$ | Shift-axis Lognormal | $\mu = 3.132, \sigma = 0.471, \theta = -3.635$ |
| $\theta$ | Empirical distribution based on statistical data | |
| $D_{min}$ | Uniform | $a = -239.891, b = 226.663$ |
| $\alpha_0$ | Shift-axis Lognormal | $\mu = 1.632, \sigma = 1.092, \theta = 0.198$ |

Based on the distribution of input parameters, Monte Carlo simulation was conducted to obtain the typhoon hazard curve, as shown in Fig. 4. The hazard curve falls within the wind speed range of a 50-year return period for the Shandong Peninsula, as reported in [45], but skews toward the upper end, indicating that the offshore area of Yantai is more susceptible to typhoon impacts.

The MCMC method was employed for Bayesian inference of model parameters to investigate the uncertainty in the typhoon hazard curve. Observational data were obtained from ERA5 within the study area and matched to typhoon impact periods, assuming that the wind field solely drives extreme wind speeds during typhoon passages. The inverse uncertainty quantification was performed for the parameters $\alpha$, $k$, $K$, and $n$, with prior distributions given in Table 2 and a likelihood function based on a normal distribution. A total of 40 MCMC chains were run for 400 iterations, discarding the first 2,000 samples as burn-in to achieve a stable posterior distribution, as shown in Fig. 5 and Fig. 6.

The posterior distributions of the parameters were sampled using Monte Carlo methods, and the model was rerun to propagate uncertainty. The resulting hazard curve, including the mean and the 95% confidence interval, is shown in Fig. 7. In the low probability range, the uncertainty of the curve significantly increases.

Table 2. A priori distribution of Batts wind field model parameters

| Parameters | Distribution | Reference |
|---|---|---|
| $\alpha$ | Uniform, [6.93,6.97] | [27] |
| $k$ | Uniform, [0.5,0.7] | [46] |
| $K$ | Uniform, [3.015, 8.08] | [32] |
| $n$ | Uniform, [0.595, 0.7] | [32] |

### 2. *Tornado*

In the tornado hazard analysis, the probability distributions of tornado path length $W_t$, path width $L_t$, maximum horizontal wind speed $U_{max}$, the ratio of tangential to radial wind speed $\gamma$, and the radius of maximum wind speed $R_{max}$ under different $F_i$ intensity levels are assumed to follow uniform distributions, as shown in the Table 3. The statistical data on tornado occurrences are based on 116 events recorded in the Shandong Peninsula from 1950 to 2013, as reported in references [36]. Among these, 35 were classified as F0, 72 as F1, and nine as F2, with no recorded tornadoes exceeding F2 intensity. The statistical region covers an area of 33,050.57 km$^2$.

Table 3. Tornado input parameter distributions by Fujita scale

| F | $L_t$ (mi = 1609 m) [25] | $U_{max}$ (m/s) [25] | $\gamma$ [35] | $R_{max}$ (m) [35] |
|---|---|---|---|---|
| 0 | [1.0, 1.8] | [25, 33] | | |
| 1 | [2.3, 3.1] | [33, 49] | | |
| 2 | [3.9, 4.7] | [49, 69] | [0.1, 0.6] | [30, 50] |
| 3 | [5.8, 6.6] | [69, 92] | | |
| 4 | [8.0, 8.8] | [93, 116] | | |
| 5 | [10.6, 11.8] | [116, 142] | | |

Considering the uncertainty in the tornado scale due to direct classification errors and random encounter errors, it is assumed that the deviation between the estimated wind speed and the actual wind speed follows a normal distribution, with a coefficient of variation ranging from 25% for F0 tornadoes to 15% for F5 tornadoes. The conditional probability matrix for random encounters is adapted from reference [39], with a correction applied to a recorded error in the matrix value of 0.0201, which was adjusted to 0.201 to ensure the sum of conditional probabilities equals one. The resulting overall conditional probability matrix is shown in Fig. 8. Under the cur-

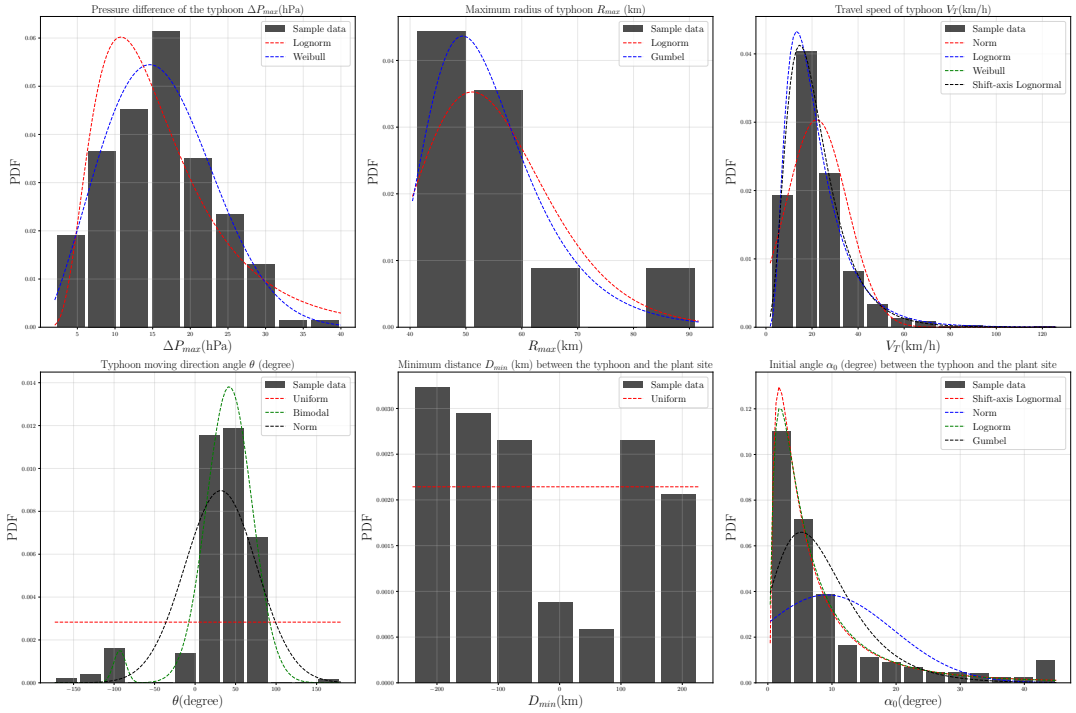


Fig. 3. Typhoon model input parameter distribution based on historical statistics

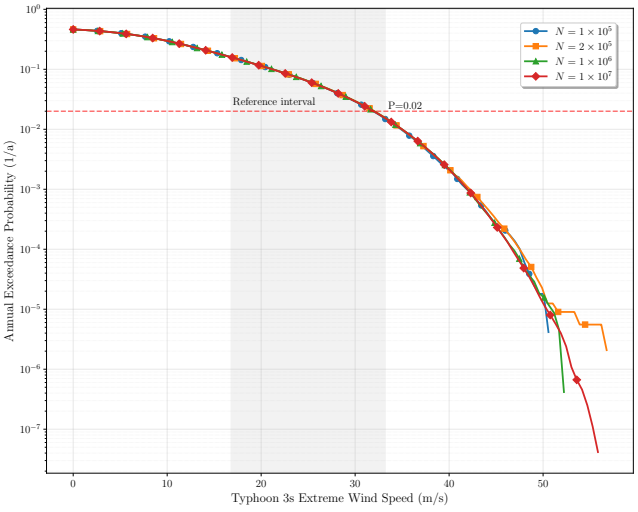


Fig. 4. Typhoon Hazard Curve

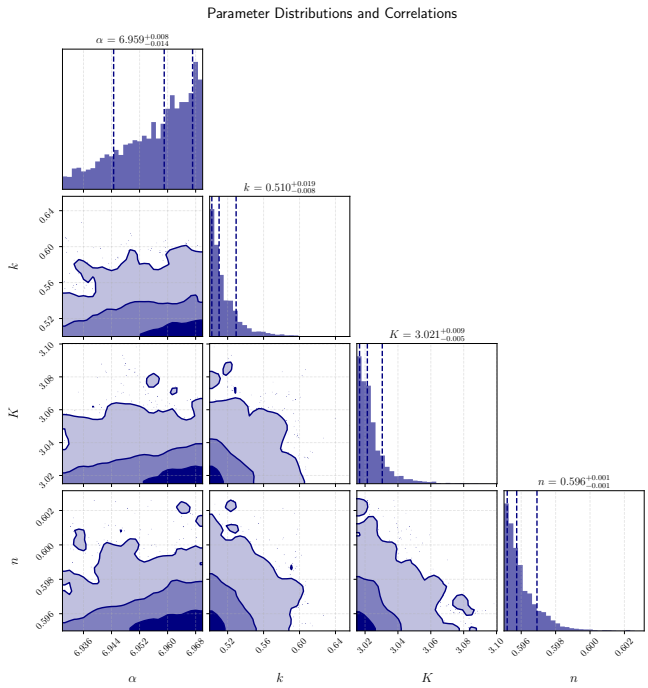


Fig. 5. Batts model parameter posterior distribution

rent assumptions, it is evident that due to random encounter errors and classification errors, tornado intensities are generally overestimated except for F0 tornadoes. However, F1 and above tornadoes may be underestimated due to insufficient observation and reporting. This conclusion is consistent with findings in references [47, 48].

Using Eq. (20), the posterior estimates of tornado intensity are shown in Fig. 9, while the final tornado hazard curve and its associated uncertainty are presented in Fig. 10. Compared to the tornado hazard analysis based on the empirical Fujita method in the literature [36, 43, 44], the hazard curve from previous studies [36] mainly falls within the 95% confidence interval of this analysis. However, the Monte Carlo simulation-based approach provides additional quantification

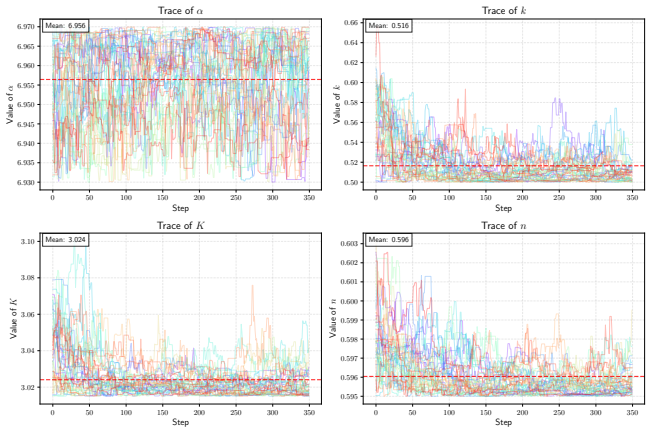


Fig. 6. Batts model parameter MCMC sampling chain

of uncertainty.

### 3. *Straight-line wind*

The straight-line wind hazard curve is derived from the fitting of observational data. Using 32 walkers, a 5000-step MCMC sampling was performed to obtain the posterior distribution of the fitted parameters, as shown in Fig. 11. The resulting straight-line wind hazard curve and its associated uncertainty are also presented in Fig. 11. Most of the observed data fall within the 95% confidence interval of the hazard curves fitted using the Gumbel and Weibull distributions.

### 4. *Combined hazard curve*

Based on the analysis results of the typhoon, tornado, and straight-line wind hazards at the factory site, the combined wind hazard curve of the site can be obtained from Eq. (19), as shown in Fig. 12. Straight-line winds dominate the low-speed range of the combined hazard curve, typhoons dominate the mid-speed range, and tornadoes govern the high-speed range. The 95% confidence interval for the extreme wind speed corresponding to a 100-year return period is [35.7, 36.2] m/s, which can be used to determine the design-basis wind load. The extreme wind speed range at an annual exceedance probability of $10^{-7}$ is [60.3, 89.3] m/s, indicating significant uncertainty.

## IV. CONCLUSION

This study developed a strong wind hazard assessment methodology tailored for floating nuclear power plants, serving as a critical component and foundation for probabilistic safety assessment (PSA) under extreme wind conditions. By integrating multi-source meteorological datasets, we derived hazard curves for straight-line winds, typhoons, tornadoes, and their combinations using wind field models, extreme value theory, and Markov Chain Monte Carlo (MCMC)-Bayesian methods. Unlike previous studies, this work quantifies uncertainties in hazard curves by presenting them with 95% confidence intervals. These results can be design-basis external event analyses for floating nuclear power plants.

Uncertainty analysis reveals that parameters of typhoon wind field models and fitting parameters for extreme value distributions of straight-line winds are significant sources of uncertainty. Tornado hazard curves exhibit higher uncertainties due to the lack of direct observational records and strong reliance on empirical correlations. Improvements in high-quality meteorological data and refined wind field models are expected to reduce these uncertainties.

As subsequent parts of the wind-related PSA, assessments of SSC fragility, plant-level PSA modeling, and quantitative evaluation will be conducted in future studies based on the current hazard analysis results.

## V. BIBLIOGRAPHY

[1] Y.X. Chen, C.H. Zhu, J. Guo et al., Preliminary study of general design of floating nuclear power plants. Nucl. Power Eng. **42**(3), 171-177 (2021). doi:10.13832/j.jnpe.2021.03.0171

[2] P.S. Antipin, A.M. Bakhmet'ev, I.E. Efimkina et al. Probabilistic safety analysis of nuclear installations of different types and classes. At. Energy. **129**, 46–49 (2020). doi:10.1007/s10512-021-00710-1

[3] Y. Liu, Z.W. Zhao, Y.C. Wang et al., Dynamic response of a multi-point mooring cylindrical floating nuclear power platform carrying a small-scale reactor. Ocean Eng. **267** (2023). doi:10.1016/j.oceaneng.2022.113121

[4] H.X. Li, Y. Wang, Y. Huang et al., Optimal design of positioning system for floating nuclear power platform in icy areas. J. Harbin Eng. Univ. **42**(2), 193-199 (2021). doi:10.11990/jheu.201910058

[5] L.X. Gong, Q.Z. Liang, C.H. Peng, PSA study of the effect of extreme snowfall on a floating nuclear power plant: case study in the Bohai Sea. Nucl. Sci. Tech. **34** (179) (2023). doi:10.1007/s41365-023-01335-8

[6] K. Lee, K.H. Lee, J.I. Lee et al., A new design concept for offshore nuclear power plants with enhanced safety features. Nucl. Eng. Des. **254**, 129-141 (2013). doi:10.1016/j.nucengdes.2012.09.011

[7] M.G. Kim, K.H. Lee, S. G. Kim et al., Conceptual studies of construction and safety enhancement of ocean SMART mounted on GBS. Nucl. Eng. Des. **278**, 558-572 (2014). doi:10.1016/j.nucengdes.2014.08.014

[8] J.X. Xiao, X.Y. Xu, H. Zhang et al., A method for hazard analysis of a floating nuclear power plant subjected to ship collision. Ann. Nucl. Energy **190**, 109870 (2023).

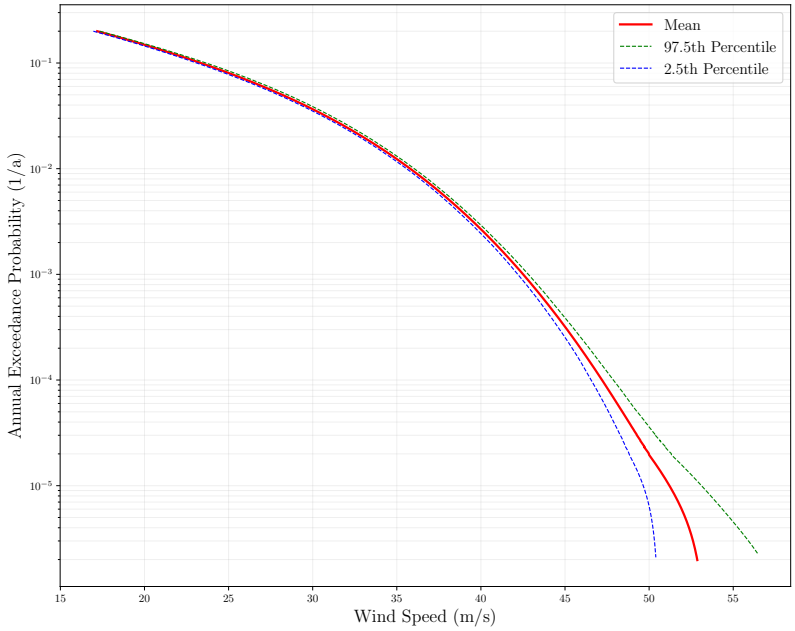


Fig. 7. Typhoon hazard curve and uncertainty

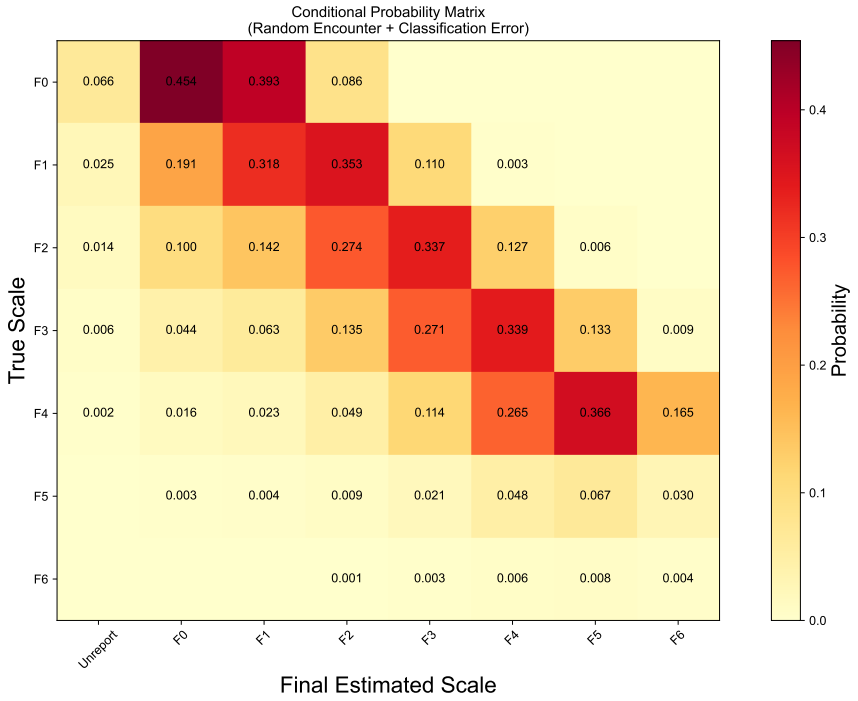


Fig. 8. Conditional probability matrix for tornado scale assessment


doi:10.1016/j.anucene.2023.109870

[9] X. Jie, Research progress of reactor thermal-hydraulic characteristics under ocean conditions in China. Front. Energy Res. **8** (2020). doi:10.3389/fenrg.2020.593362

[10] Y. Wu, S. Yu, Y. Liu, Three-level assessment of the safety of floating nuclear power plants under hazard waves. in *Paper presented at 2023 Global Reliability and Prognostics and Health Management Conference*, *Hangzhou*, *China*, (12-15 October 2023). doi:10.1109/PHM-Hangzhou58797.2023.10482585

[11] Y. Huang, X. Song, S. Zou et al., Study on the atmospheric diffusion of airborne radionuclide under LOCA of offshore floating nuclear power plants based on CALPUFF. Sustainability **15**, 2572 (2023). doi:10.3390/su15032572

[12] Y. Ko, H. Seo, H. K. Cho et al., SBLOCA analysis of a float-

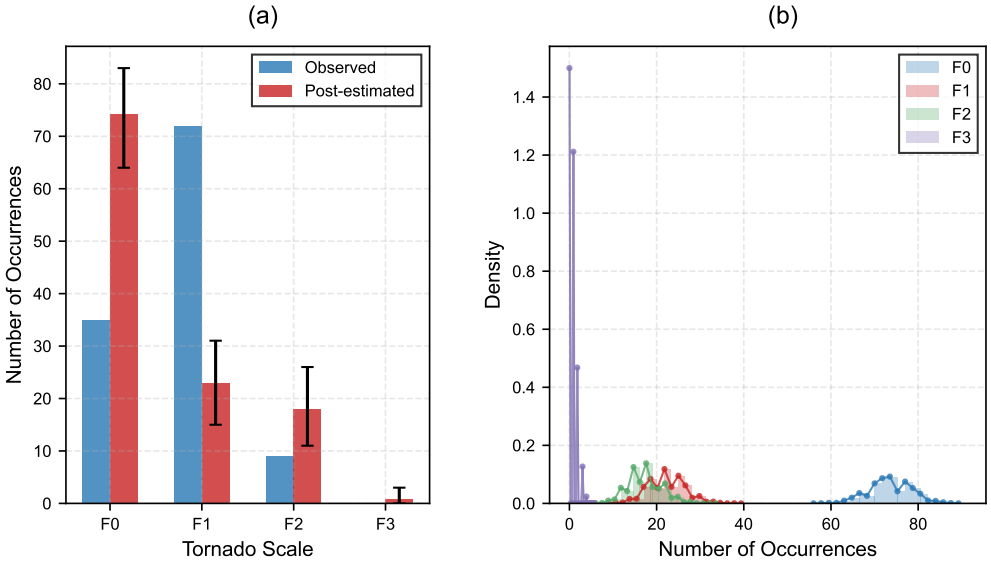


Fig. 9. Tornado intensity posteriori estimation

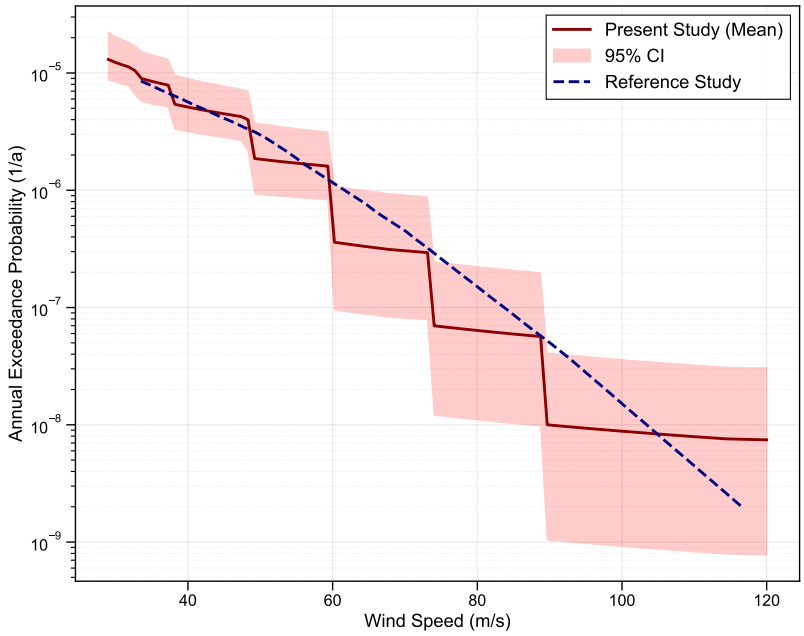


Fig. 10. Tornado hazard curve and uncertainty

ing nuclear reactor under ocean conditions using MARS-KS moving reactor model. Prog. Nucl. Energy **168**, 105017 (2024). doi:10.1016/j.pnucene.2023.105017

[13] M. Behzadi, M. Abbasi, A. Zolfaghari et al., Analysis of two-phase flow in non-inertial coordinate using combination of three-fluid model and drift flux model. Prog. Nucl. Energy **151**, 104334 (2022). doi:10.1016/j.pnucene.2022.104334

[14] G. Guan, S.G. Du, B.Y. Huang et al., Study on the mechanical behavior of penetrations in floating nuclear power plants under ocean swing load. Ann. Nucl. Energy **214**, 111224 (2025). doi:10.1016/j.anucene.2025.111224

[15] T. Xu, J. Wang, B. Zhang et al., Research on diffusion and mitigation of severe accident source terms in floating nuclear power plant. in *Paper presented at Proceedings of the 31st International Conference on Nuclear Engineering*, *Prague*, *Czech*, (4–8 August 2024). doi:10.1115/ICONE31-139205

[16] M.C. Maturana, D.T.M. Pereira Abreu, M.R. Martins et al., Application of technique for early consideration of human reliability in the specification of the maximum acceptable probability of failure on demand and the maximum spurious operation frequency of a floating nuclear power plant safety control system. in *Paper presented at ASME 42nd International Conference on Ocean, Offshore and Arctic Engineering*, *Melbourne*, *Australia*, (11-16 June 2023).

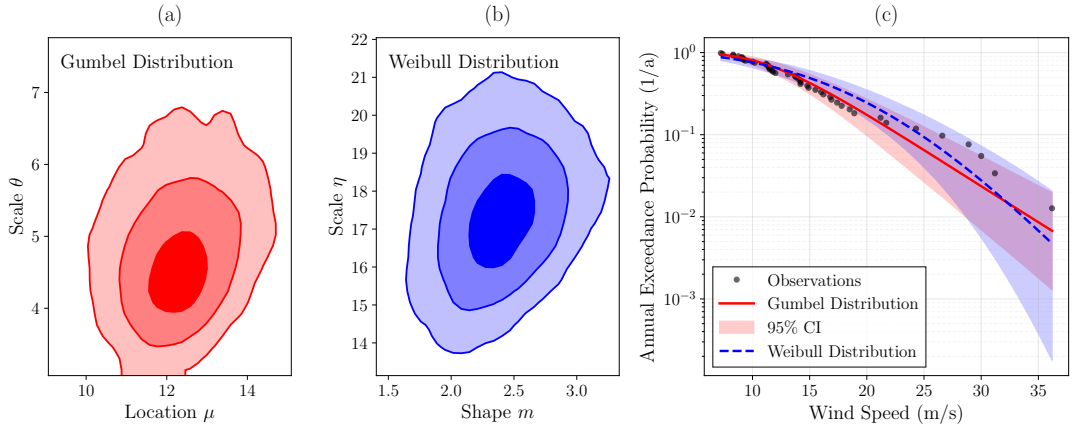


Fig. 11. Straight wind hazard curve and uncertainty

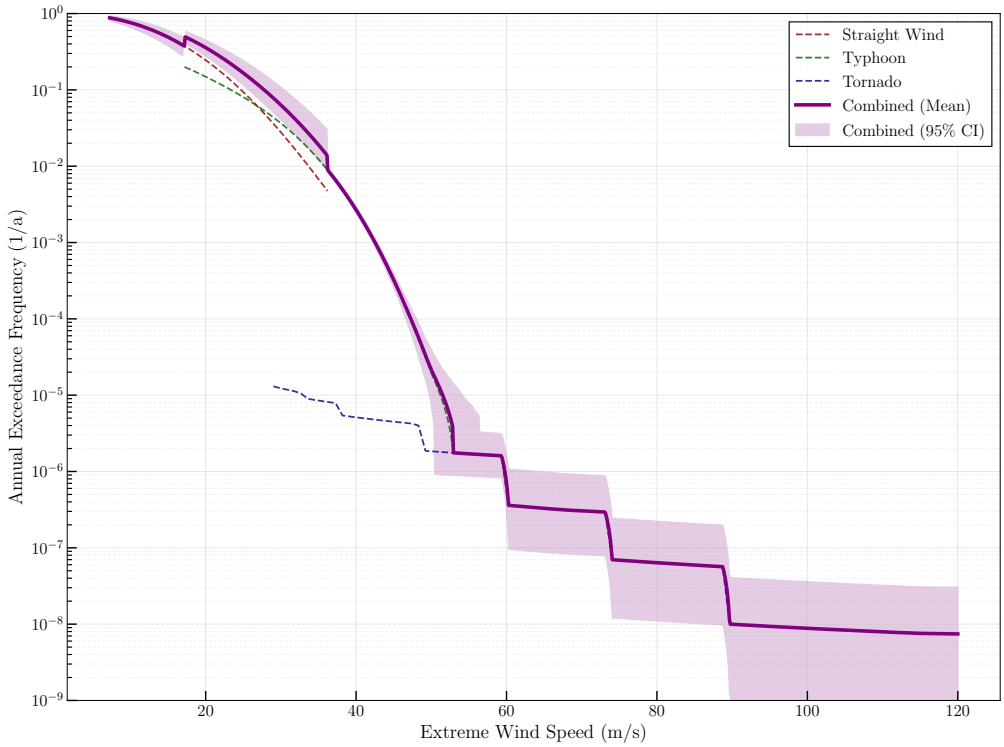


Fig. 12. Combined wind hazard curve and its uncertainty


doi:10.1115/OMAE2023-104971

[17] C. Yin, H. Li, X. Xie et al., Study of reliability prediction method and uncertainty analysis of the pump and valve of a floating nuclear power plant. Kerntechnik **89**(6), 701-716 (2024). doi:10.1515/kern-2024-0103

[18] S. Zou, B. Huang, Y. Kuang, Reliability analysis and evaluation of the key equipment of the marine floating nuclear power plants based on the left-right fuzzy ranking. J. Saf. Environ. **20**(4), 1248-1254 (2020). doi:10.13637/j.issn.1009-6094.2019.0502

[19] Y.B. Vorobyev, D.S. Urtenov, V.E. Karnaukhov et al., Consideration of uncertainties in analyzing nuclear power facilities' fire hazard. Therm. Eng. **67**, 640–646 (2020). doi:10.1134/S0040601520090098

[20] S.S. Fu, Y.R. Yu, J.H. Chen et al., Towards a probabilistic approach for risk analysis of nuclear-powered icebreakers using FMEA and FRAM, Ocean Eng. **260**, 112041 (2022). doi:10.1016/j.oceaneng.2022.112041

[21] K. Izmail, Extreme design storms for floating nuclear power plant projects. RT&A **6**(81) (2024).

[22] N. Hiroyuki, K. Kenichi, Y. Hidemasa, Development of risk assessment methodology of decay heat removal function against external hazards for sodium-cooled fast reactors (2) probabilistic risk assessment methodology against strong wind. in Paper *presented at Proceedings of 23th International Conference on Nuclear Engineering*, *Chiba*, *Japan*, (17-21 May 2015).

doi:10.1299/jsmeicone.2015.23._icone23-1_61

[23] Y. Hidemasa, N. Hiroyuki, K. Kenichi, Development of a probabilistic risk assessment methodology against a combination hazard of strong wind and rainfall for sodium-cooled fast reactors. Mech. Eng. J. **5**(4), 18-00093 (2018). doi:10.1299/mej.18-00093

[24] H. Nishino, K. Kurisaka, H. Yamano, Development of margin assessment methodology of decay heat removal function against external hazards (2) tornado PRA methodology. In *Paper presented at Proceedings of the 10th international topical meeting on nuclear thermal-hydraulics, operation and safety*, *Okinawa*, *Japan*, (14–18 Dec 2014).

[25] Y.J. Park, M. Reich, Probabilistic wind/tornado/missile analyses for hazard and fragility evaluations. (Brookhaven National Laboratory, 1995), https://www.osti.gov/servlets/purl/110764. Accessed 5 March 2025.

[26] G.E. Bozoki, C.S. Conrad, Level 1 tornado PRA for the high flux beam reactor. (Brookhaven National Laboratory, 1994), doi:10.2172/48761. Accessed 5 March 2025.

[27] M.E. Batts, M.R. Cordes, C.R. Russell et al., Hurricane Windspeeds in the United States. (National Bureau of Standards, 1980), https://nvlpubs.nist.gov/nistpubs/Legacy/BSS/nbsbuildingscience124.pdf. Accessed 5 March 2025.

[28] P.J. Vickery, D. Wadhera, L.A. Twisdale et al., United States hurricane wind speed risk and uncertainty. J. Struct. Engin. **135**(3), 301–320 (2009). doi:10.1061/(ASCE)0733-9445(2009)135:3(301)

[29] P.J. Vickery, D. Wadhera, L.A. Twisdale, Technical basis for regulatory guidance on design-basis hurricane wind speeds for nuclear power plants. (United States Nuclear Regulatory Commission, 2011), https://www.nrc.gov/docs/ML1133/ML11335A031.pdf. Accessed 5 March 2025.

[30] U.S. Nuclear Regulatory Commission, Design-basis tornado and tornado missiles for nuclear power plants. (United States, 2007). https://www.nrc.gov/docs/ML0703/ML070360253.pdf. Accessed 5 March 2025.

[31] E. Simiu, A.P. Florian, Technical basis for regulatory guidance on design-basis hurricane-borne missile speeds for nuclear power plants. (United States Nuclear Regulatory Commission, 2011), https://www.nrc.gov/docs/ML1134/ML11341A102.pdf. Accessed 5 March 2025.

[32] X.L. Li, Z.D. Pan, J. She, A Method for Adjustment of Typhoon Parameters. J. Oceanogr. Huanghai Bohai Seas **2**, 11-15 (1995).

[33] E. Simiu, D.H. Yeo, *Wind Effects on Structures: Modern Structural Design for Wind*, 4th edn. (Wiley, 2019), pp. 27

[34] A. Ghosh, S. Rafkin, Review of methods for estimation of high wind and tornado hazard frequencies. (U.S. Nuclear Regulatory Commission, 2012). https://www.nrc.gov/docs/ML1930/ML19305C919.pdf. Accessed 5 March 2025.

[35] W.L. Dunn, L.A. Twisdale, A synthesized windfield model for tornado missile transport. Nucl. Eng. Des. **52**(1), 135-144 (1979). doi:10.1016/0029-5493(79)90015-3

[36] H.B. Liu, Shandong peninsula regional tornado and its destructive power parameter character. in *Paper presented at Proceedings of China Meteorological Society 2005 Annual Conference*, *Suzhou*, *China*, (October 2005).

[37] L. Gomes, B.J. Vickery, Extreme wind speeds in mixed wind climates, J. Wind Eng. Ind. Aerodyn. **2**(4), 331-344 (1978). doi:10.1016/0167-6105(78)90018-1

[38] J.Q. Zeng, H.X. Zhang, H.L. Gong et al., Ensemble Bayesian method for parameter distribution inference: application to reactor physics. Nucl. Sci. Tech. **34**, 199 (2023). doi:10.1007/s41365-023-01356-3

[39] E. Simiu, Tornado missile simulation and design methodology. (Electric Power Research Institute, 1983), https://www.nrc.gov/docs/ML2008/ML20080C454.pdf. Accessed 5 March 2025.

[40] M. Ying, W. Zhang, H. Yu et al., An overview of the China meteorological administration tropical cyclone database. J. Atmos. Oceanic Technol. **31**, 287-301 (2014). doi:10.1175/JTECH-D-12-00119.1

[41] X.Q. Lu, H. Yu, M. Ying et al., Western north Pacific tropical cyclone database created by the China meteorological administration. Adv. Atmos. Sci. **38**(4), 690-699 (2021). doi:10.1007/s00376-020-0211-7

[42] J. Muñoz Sabater, ERA5-Land hourly data from 1950 to present. (Copernicus Climate Change Service (C3S) Climate Data Store (CDS), 2019), doi:10.24381/cds.e2161bac. Accessed 5 March 2025.

[43] W.J. Fan, X.D. Yu, Characteristics of spatial temporal distribution of tornadoes in China. Meteor Mon. **41**(7), 793-805 (2015). doi:10.7519/j.issn.1000-0526.2015.07.001

[44] Y.F. Sun, D.Y. Li, J.X. Wang et al., Temporal-spatial statistical characteristics and disaster analysis of tornadoes in China. Front. Earth Sci. **14**(7): 935-948 (2024). doi:10.12677/ag.2024.147087

[45] H.B. Liu, M.F. Wu, Analysis of high impact meteorological conditions of coastal wind farms in northern Shandong. Open J. Nat. Sci. **9**(5), 723-731 (2021). doi:10.12677/ojns.2021.95078

[46] A.A. Richard,*Tropical cyclones: Their evolution, structure and effects*, 1st edn. (American Meteorological Society Boston, MA, 1982), pp. 22

[47] C.K. Potvin, C. Broyles, P.S. Skinner et al., Improving estimates of U.S. tornado frequency by accounting for unreported and underrated Tornadoes. J. Appl. Meteor. Climatol. **61**, 909–930 (2022).doi:10.1175/JAMC-D-21-0225.1

[48] C. K. Potvin, C. Broyles, P.S. Skinner et al., A Bayesian hierarchical modeling framework for correcting reporting bias in the U.S. tornado database. Wea. Forecasting **34**, 15–30 (2019). doi:10.1175/WAF-D-18-0137.1